2nd International Symposium on Magnetic Beaing
July 12-14, 1990, Tokyo, Japan

PERMANENT MAGNET BIASED MAGNETIC BEARINGS – DESIGN, CONSTRUCTION AND TESTING

Christopher K. Sortore, Engineer, Aura Systems, El Segundo, CA 90245
Paul E. Allaire, Assistant Dean and Professor, Mech. & Aero. Engr., Univ. of Virginia, Charlottesville, VA 22901
Eric H. Maslen, Graduate Research Assistant, Mech. & Aero. Engr., Univ. of Virginia, Charlottesville, VA 22901
Robert R. Humphris, Research Professor, Mech. & Aero. Engr., Univ. of Virginia, Charlottesville, VA 22901
Phil A. Studer, Private Consultant, Magnetic Concepts, Silver Spring, MD 20901

Abstract

Magnetic bearings may have the steady state bias flux supplied either from electromagnet coil currents or from permanent magnets. In the second case, the active control flux is provided by electromagnetic coils. The permanent magnet bias design provides advantages of minimum power consumption, smaller size and weight compared to the all electromagnetic design. This paper outlines the theoretical analysis of permanent magnet biased magnetic bearings. Further, it describes the construction and testing of a set of these bearings in a high speed rotor test rig. The bearings were tested in a rotor in several ways, including white noise excitation (non–rotating) and unbalance response (rotating) up to 23,000 rpm. Theoretical and measured results are compared. The power consumption of the original liquid lubricated bearings was 3,000 watts while the all electromagnetic design was approximately 500 watts. The permanent magnet biased design was measured at 207 watts (total power).

Nomenclature

a	area	F	Laplace trans. force
f	force vector	H	mag. field strength
g	air gap length	I	current
k_{eq}	equiv. stiffness	J	current density
k_i	actuator gain	N	no. of wire turns
k_x	bearing stiffness	W	energy
l	mag. path length	∇	gradient operator
s	Laplace variable	μ_0	mag. permeability of free space
$\underline{s}$	position	μ_r	rel. permeability
v	volume	∇	gradient operator
B	mag. induction		

1. Introduction

Magnetic bearings have advanced to the point of being able to offer several different varieties of advantages to rotating machinery manufacturers and users. The use of permanent magnets, in conjunction with electromagnets, provides one appealing option which strongly reduces the power required to operate magnetic bearings. Power consumption reduction of at least an order of magnitude is expected over conventional bearings.

Studer [1] discussed the use of magnetic bearings for space use in an energy storage flywheel. Many other researchers, such as Murakami, et. al [2], Heimbold [3], and Eisenhaure [4], to cite only a few, have explored the use of magnetic bearings in space. Work on flexible shaft rotating machines has been reported by Allaire et. al [5, 6]. Keith et. al [7] and Yates et. al [8] developed a digital control systems for magnetic bearings in high speed rotating machines.

Permanent magnets have been successfully employed in passive magnetic bearings by Yonnet [9] and Okuda et. al [10]. These bearings have the advantage of eliminating the weight and complexity of the electromagnetic components of the combination bearings. However, these bearings have low damping characteristics and the dynamic stability is less than required in some situations as reported by Arai [11].

Two early patents were obtained by Studer [12,13] on the use of permanent magnets in magnetic bearings. These patents have useful concepts similar to those employed in the bearings discussed in this paper. Wilson and Studer [14] have applied the permanent magnet bias concept to linear motion bearings. Ohkami et. al [15] have performed some interesting comparative studies of magnetic bearings which use permanent magnet biasing. Tsuchiya et. al [16] studies the stability of a high speed rotor suspended in magnetic bearings. Meeks [17] has performed a comparison of various magnetic bearing design approaches and concludes that combining actively controlled electromagnets with permanent magnets results in a superior magnetic bearing in terms of size, weight and power consumption.

This work describes the design, construction and testing of a set of magnetic bearings using this concept [18]. Both permanent magnets and electromagnets are used in a configuration which effectively provides the necessary flux in the appropriate air gaps, while simultaneously keeping the undesirable power losses to a minimum. The design includes two radial bearings and a thrust bearing.

2. Magnetic Bearings

The first bearing discussed is the radial bearing. It operates at one end of the high speed rotor (described later) and controls radial forces only. Two views of this bearing are shown in Figure 1. Appendix A presents an analysis of a simplified magnetic circuit with a permanent magnet providing the bias flux. Four axially magnetized arc segments are positioned circumferentially adjacent to the rotor. The bias flux generated by the permanent magnets passes down the laminated stator pole leg, through the working air gap, axially along the shaft, then returns to the permanent magnet via a radial bias pole piece. The active control generated by the coils also passes down the stator pole leg and through the working air gap.

The return path for the active (control) flux is different. It flows circumferentially around the stator, as shown in Figure 1. This design thus requires only four poles and four coils, in contrast to the all electromagnetic designs. Appendix A gives a discussion of the theory associated with the bearing design. Additionally, the coils for each bearing axis are connected in series. This means that the bearing control system requires only five current amplifier channels rather than the ten required of the all electromagnetic design.

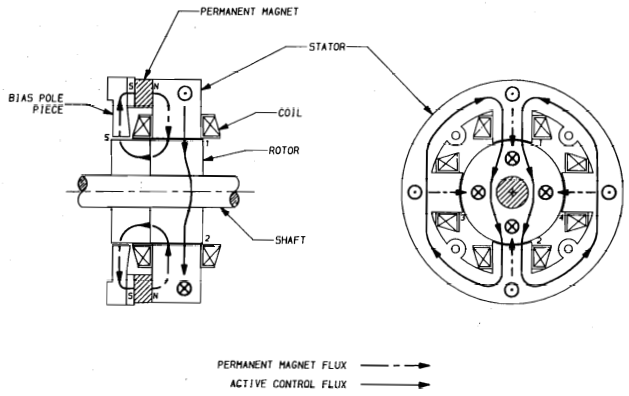

Fig. 1 Radial Magnetic Bearing Flux Paths

The combination radial/thrust bearing is illustrated in Fig. 2. The radial portion of the bearing is very similar to the radial bearing at the other end. However, the thrust bearing has a unique magnetic flux path design. The permanent magnet bias flux passing along the shaft splits equally between the two thrust poles before returning to the permanent magnet. A single active (control) coil produces a magnetic flux, in the shape of a toroid, which adds or subtracts to the bias flux in the working air gaps between the thrust disk and the thrust poles.

The bearings designed for this project are different from all electromagnetic bearing designs in that they employ both permanent magnets and electromagnets. Permanent magnets generate the bias flux in the working air gaps and electromagnets are used to modulate this flux.

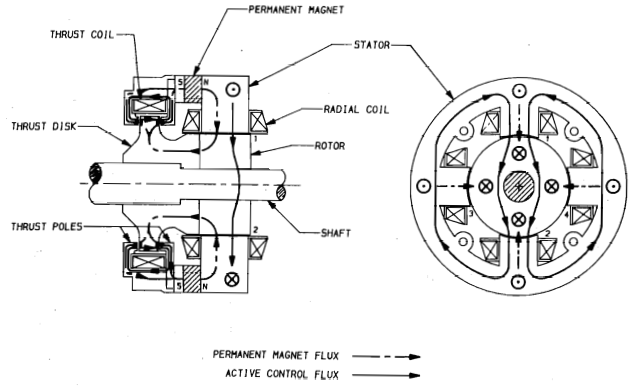

Fig. 2 Combination Radial/Thrust Magnetic Bearing Flux Paths

The purpose of establishing a bias flux in the working air gaps is to linearize the governing force equation of the magnetic actuator. The bias flux is a nominal flux density about which the control flux is varied. If a bias flux of zero is used (only one opposing actuator is operated at a time), then the force generated by the actuator on the rotor follows a quadratic force law, i.e., the force will be proportional to the square of the flux density in the air gaps. Consequently, the force slew rate will be zero when the rotor is in the nominal balanced position and the transient response will be adversely effected. If, however, the bearing fluxes are modulated about a non–zero bias flux, (with opposing actuators symmetrically perturbed) it is easily shown that the force becomes linearly related to the control flux. The following section demonstrates this important relation.

3. Bearing Forces

The force generated by a magnetic bearing on an object suspended in its field is a function of the geometry of the magnetic circuit and the magnetic induction in its air gaps. For simple magnetic circuits, this function is also quite simple. In the classic bearing geometry where an object is suspended between two opposing horseshoes, the force acting on the suspended body is given by the simple relation

$$f = \frac{A_g}{\mu_o}(B_1^2 - B_2^2) \tag{1}$$

If these two flux densities are perturbed symmetrically about some fixed point, then the resulting force is linear in the perturbation flux. That is if

$$B_1 = B_{bias} + B_{pert} \tag{2}$$

and

$$B_2 = B_{bias} - B_{pert} \tag{3}$$

then the net force is given by

$$f = 4\,\frac{A_g}{\mu_o}\,B_{bias}\,B_{pert} \tag{4}$$

Equation (4) illustrates the linearizing effect of a bias flux. An important fact concerning this bias flux is that it is to be held constant: modulation of the bearing force is accomplished by modulating a superimposed perturbation or control flux.

The purpose of introducing permanent magnets into a magnetic bearing circuit is to establish this bias flux without using any energy. The trick is to do this without requiring the control flux to pass through the permanent magnets, which have a low permeability.

The various magnetic circuits which have been devised to accomplish this combination of permanent magnet biasing and electromagnet perturbation tend to be more complicated than the simple opposing horseshoe scheme described above, with the result that the equations governing their generated forces are more complicated than (1). One method for determining the operating equations is based on studying the variation of the magnetic energy in the circuit as the supported object

is moved. Appendix A outlines such a method. The main result of the energy analysis is that the force in any given direction is approximated by

$$f_x \cong \frac{\partial}{\partial x}\left[\frac{1}{2\mu_o}\sum_{i=1}^{gaps} B_i^2 v_i\right] \qquad (5)$$

Although the actual operating equations are more complicated than (1), they retain the main result that the operation of the bearing is linearized by prebiasing the air gaps to a fixed level and then perturbing them symmetrically.

4. Open Loop Stiffness and Actuator Gain

The force generated by a magnetic bearing is generally described by an equation which is linear in the control current but is most likely nonlinear in the displacement of the supported object. For the purpose of studying the stability and dynamic performance of the closed loop system, a linearized actuator mathematical model of the magnetic bearing is required. The bearing force acting in the x direction is expanded in a truncated Taylor series as

$$f_x(x,i_c) = f_x\Big|_{\substack{x=0\\ i_c=I_o}} + \frac{\partial f_x}{\partial x}\Big|_{\substack{x=0\\ i_c=I_o}} x + \frac{\partial f_x}{\partial i_c}\Big|_{\substack{x=0\\ i_c=I_o}} (i_c - I_o) \qquad (6)$$

where I_o is the nominal control current required to hold the object suspended at x=0. In the absence of body forces and with a perfectly balanced circuit, this current will usually be zero. Since I_o is the current required to suspend the object at x=0, the net force acting on the object is

$$f_{x_{net}} \cong \frac{\partial f_x}{\partial x}\Big|_{\substack{x=0\\ i_c=I_o}} x + \frac{\partial f_x}{\partial i_c}\Big|_{\substack{x=0\\ i_c=I_o}} (i_c - I_o) \qquad (7)$$

The linearized actuator properties are identified from (7) as

$$K_x \equiv -\frac{\partial f_x}{\partial x}\Big|_{\substack{x=0\\ i_c=I_o}} \quad \text{and} \quad K_i \equiv \frac{\partial f_x}{\partial i_c}\Big|_{\substack{x=0\\ i_c=I_o}} \qquad (8)$$

The minus sign in the definition of K_x is introduced so that this term can be described as a stiffness. In the absence of a feedback loop, the stiffness of the support is entirely governed by K_x, so this term is referred to as the open loop stiffness. K_x is negative, indicating the open loop instability of magnetic suspensions. K_i relates the actuator force to the control current, so it is called the actuator gain.

Similar expressions can be obtained for each of the other two orthogonal directions. For a radial bearing, the axial properties are usually very weak and are ignored, and, likewise for a thrust bearing, the radial components are typically ignored.

5. Control System

The control circuitry is the key to any stable magnetic bearing system. This segment detects the motion of the shaft, determines the necessary control force and then supplies a current to the appropriate electromagnet to generate this force. Four distinct components make up the magnetic bearing system: 1) the magnetic actuators, 2) the position probes and associated conditioning circuitry, 3) analog proportional–integral–derivative (PID) controllers and 4) transconductance power amplifiers.

The actuator of the magnetic bearing is comprised of coils, iron stator pole pieces, permanent magnets and the rotor. The position probes are eddy current induction sensors and their output signals pass through coordinate transformation circuits to the analog controller, which contains the PID compensation network. The output of this compensator drives the transconductance power amplifier. This amplifier supplies the necessary current to the various coils, which produce the required magnetic fluxes and forces for stable operation of the bearing.

The operational behavior of the control electronics may then be combined with the dynamics of the bearing–rotor system to form the overall closed–loop control system. Figure 3 shows a block diagram of such a system. The characteristics of the position sensor, PID analog controller and the power amplifier are all combined in the complex transfer function, $G_c(s)$, of the feedback controller. This transfer function, $G_c(s)$, relates the rotor position to the actuator current. From the block diagram, the approximate closed–loop transfer function is determined to be

$$\frac{X(s)}{F_x(s)} = \frac{1}{ms^2 + K_x + K_i G_c(s)}$$

where m is the effective mass of the rotor.

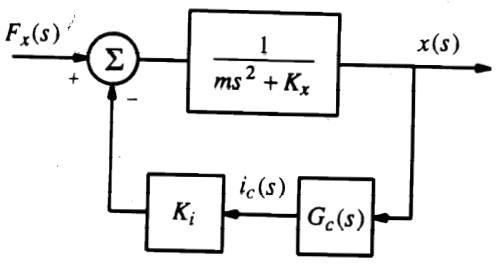

Fig. 3 Closed Loop Magnetic Bearing Control System

6. Prototype Bearing Construction

The four–pole radial bearing stator, shown in Figures 1 and 2, is designed to be identical for both bearings. The stators and rotors are constructed of a silicon–iron lamination material of 0.18 mm (0.007 inches) thickness. Each rotor and stator consists of

approximately 100 laminations, which were glued together using a two part activator/resin adhesive. The final shapes were machined by wire EDM (electric discharge machining). The bearing stators have an outside diameter of approximately 10.6 cm (3.0 inches) with an axial length of 1.8 cm (0.7 inches). The outside diameter of the laminated rotor is 3.8 cm (1.5 inches). Thrust bearing components were machined from soft magnet iron. The high energy permanent magnets, made from a Neodymium–Iron–Boron alloy, have a maximum energy product of 2.4 x 10^5 T–Amps/m (30 MG–Oe). The bearings support a shaft weighing approximately 1.68 kG (3.7 lbm).

7. Load Capacity

Results of measurements of the maximum load applied to the shaft, before it falls out of support, are plotted as a function of the controller proportional gain, K_P, in Figure 4. For these measurements the force was applied to the shaft by hanging weights and a pulley system constructed such that the force was acting in the appropriate direction, i.e. along the bearing axes.

The variation of the maximum load at lower proportional gains is actually a measure of the stability threshold of the system. As noted earlier, the open loop stiffness, K_x, is defined at a nominal operating point, i.e. rotor position deviation and control current are equal to zero. However, as the bearing is loaded with a static force, the steady state current begins to increase and it can be shown that K_x is a function of the operating point of the control current. In other words, as the control current increases, K_x also increases and thus increasing the proportional gain has the effect of compensating for this increase in K_x and consequently improving the stability of the system.

Therefore, measurements made at the higher proportional gains represent a more accurate indication of the actual load capacity of the bearing, whereby sufficient stability is provided so that magnetic saturation of the pole structures is achieved. The maximum predicted loads shown in Figure 4 are calculated using a saturation flux density value.

8. Equivalent Bearing Stiffness and Damping

Results of measurements of the equivalent stiffness of the radial and thrust bearings are shown in Figure 5. A constant force, ΔF, was applied and the displacement, Δx, of the shaft was noted while the controller integrators were switched off. The stiffnesses may then be easily found from $K_{eq} = \Delta F/\Delta K$. A linear regression, performed on the measured data, indicated a very good correlation to predicted values. It should be noted that the proportional gain, K_P, has a direct effect on the stiffness of the bearings, as previously demonstrated by Humphris, et al. [19].

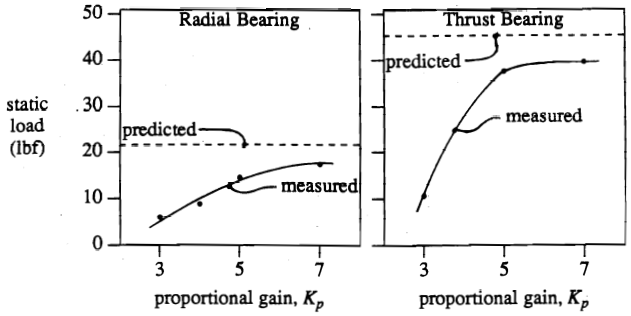

Fig. 4 Load Capacity versus Proportional Gain Setting

Relative damping in the bearings was investigated by analyzing the frequency response of the rotor to injected white noise. Noise composed of all frequencies of interest was injected into the power amplifier of the appropriate axis under study and a Fast Fourier Transform (FFT) was performed on the sensor output of that axis. A typical frequency response, composed of 100 averages, is shown in Figure 6 for the turbine–end radial bearing as the controller derivative gain, K_r, is varied. As expected [19], this derivative gain variation had a direct effect on the damping in the bearing. The first large peak represents the first two modes of shaft vibration, as they are very close together in frequency and essentially indistinguishable. The frequency of the observed second peak is actually the third mode of shaft vibration and the third small peak near 60,000 rpm is the fourth mode. Note that the derivative gain variation strongly affects the first two modes, has a smaller effect on the third mode and virtually no influence on the amplitude of vibration of the fourth mode.

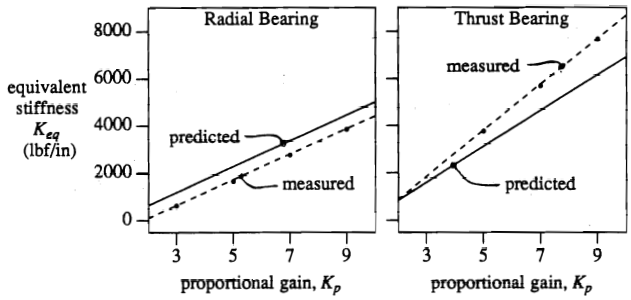

Fig. 5 Equivalent Bearing Stiffness versus Proportional Gain Settings

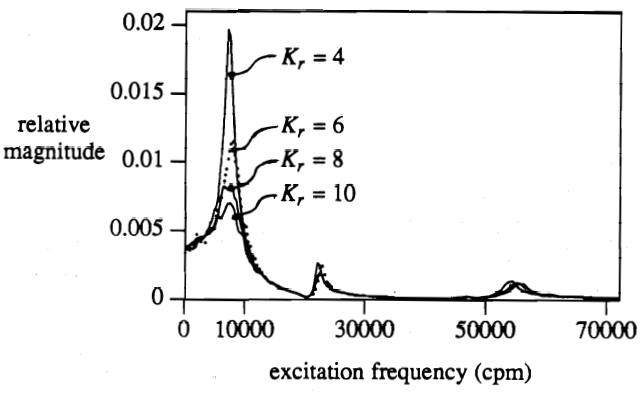

Fig. 6 Frequency Response to White Noise

9. Critical Speeds and Rotor Response

The frequency response due to white noise indicates the approximate damped critical speeds of the flexible shaft supported in magnetic bearings. However, these values represent the zero speed natural frequencies. The effects of gyroscopic stiffening due to attached disks would not be included. With the shaft rotating, the observed critical speeds would be higher, as expected, since the natural frequency is given by $\omega_n = \sqrt{k/m}$, where k is the system stiffness and m is the modal mass of the rotor. Actual run–up vibration magnitude and phase information for rotor speeds up to approximately 23,000 rpm is shown in Figure 7. High vibration levels at the onset of the third critical mode prevented operation at higher speeds. As noted in Figure 7, the first vibration mode is observed as approximately 10,000 rpm and the second at approximately 13,000 rpm.

10. Power Consumption

Finally, several power measurements on the overall magnetic bearing system were made with a wattmeter. The total power consumption for this bearing with its supporting electronics was 207 watts. This measurement represents a significant improvement over the approximately 500 watts of total power consumed by a comparable magnetic bearing using no permanent magnets.

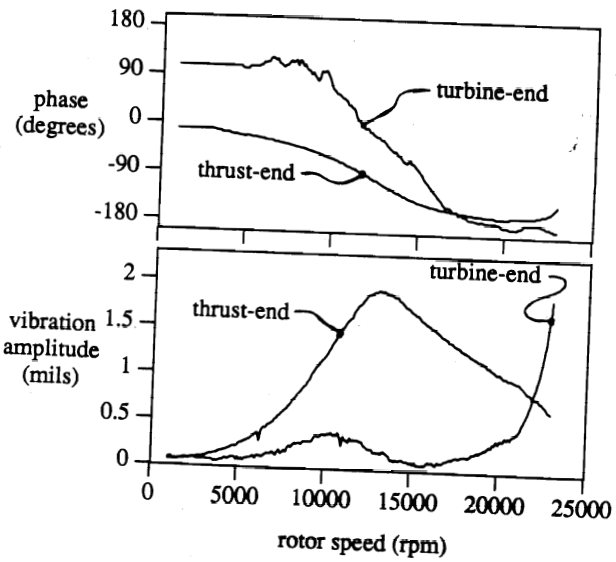

Fig. 7 Rotor Runup Response

11. Conclusions

The brief theory which was presented in this paper established the basic electromagnetic and mechanical relationships necessary to develop a set of permanent magnet biased magnetic bearings. The design involved both radial and thrust bearings. The availability of newer rare–earth high energy permanent magnets made it possible to effectively provide the necessary bias fluxes in the bearing.

The bearings and rotor were successfully constructed and operated. A number of tests and experiments were performed on the bearing–rotor system. The tests consisted of load capacity, stiffness and damping measurements. The results proved to be very positive in that the theoretical predictions and the observed performance matched reasonably well, giving credibility to the models which were used to perform the analysis. Of particular interest for this study was the measured power consumption of the bearings. It clearly demonstrates that the use of permanent magnets can improve the operating efficiency of an active magnetic bearing, in this case by a factor of 2.5.

It was successfully observed and demonstrated that these bearings have strong potential for future use as efficient, reliable bearings. However, further research and developed is required in the areas of controls, magnetic materials and actuator design before it is possible to install them into a useful industrial application.

References

1. Studer, P. A., "Magnetic Bearings for Instruments in the Space Environment," NASA Technical Memorandum 78048, 1978.

2. Murakami, C., A. Nakajima, S. Akishita, M. Inoue and K. Yabu'Uchi, "A Magnetically Suspended Flywheel for Attitude Control of Satellites," Mitsubishi Denki Giho (Japan), Vol. 58, No. 3, pp. 26–30, 1984.

3. Heimbold, G., "Impact of Magnetic Bearing Rotor Design on Satellite Nutational Stability," Journal of Guidance Control Dynamics, Vol. 7, No. 3, pp. 279–285, 1984.

4. Eisenhaure, D., "Inertial Energy Storage for Satellites," NASA Conference Publication 2346, pp. 101–116, 1984.

5. Allaire, P. E., R. R. Humphris and L. E. Barrett, "Critical Speeds and Unbalance Response of a Flexible Rotor in Magnetic Bearings," Presented at the European Turbomachinery Symposium, Brunel, The University of West London, October 1986.

6. Allaire, P. E., R. R. Humphris and R. D. Kelm, "Magnetic Bearings for Vibration Reduction and Failure Prevention," Proceedings of the 40th Meeting of Mechanical Failures Prevention Group, National Bureau of Standards, Gaithersburg, MD, April 1985.

7. Keith, F. J., R. D. Williams, P. E. Allaire and R. M. Schafer, "Digital Control of Magnetic Bearings Supporting a Multimass Flexible Rotor," Presented at the Magnetic Suspension Technology Workshop, Hampton, VA, February 1988.

8. Yates, S. W. and R. D. Williams, "A Fault–Tolerant Multiprocessor Controller for Magnetic Bearings," IEEE Micro, pp. 6–17, August 1988.

9. Yonnet, J.–P., "Passive Magnetic Bearings Made Only with Permanent Rings," Proc. 6th Int'l Workshop on Rare Earth–Cobalt Permanent Magnets and Their Applications, pp. 203–212, 1982.

10. Okuda, H. T., K. Abukawa, and M. Ito, "Charac–teristics of Permanent Magnet Bearings," Hitachi Research Laboratory, Hitachi Ltd., Japan, 1984.

11. Arai, J., "Dynamic Stability of a Passive Magnetic Suspension With an Eight–Pole Stator," Bulletin JSME, Vol. 27, No. 229, pp. 1506–1512, 1984.

12. Studer, P. A., NASA, **Magnetic Bearing**, Patent 3865442, Patent Application 100637, February 1975.

13. Studer, P. A., NASA, **Linear Magnetic Bearing**, Patent 4387935, Patent Application 214361, Dec. 1980.

14. Wilson, M. and P. A. Studer, "Linear Magnetic Bearings," Presented at the Int'l Workshop on Rare Earth–Cobalt Magnets and Their Applications, Roanoke, VA, June 1981.

15. Ohkami, Y., O. Okamato, T. Kida, C. Murakami, A. Nakajima, S. Hagihara and K. Yabuuchi, "A Comparison Study of Various Types of Magnetic Bearings Utilizing Permanent Magnets," Presented at the Int'l Workshop on Rare Earth–Cobalt Magnets and Their Applications, Roanoke, VA, June 1981.

16. Tsuchiya, K. and M. Inoue, A. Nakajima, Y. Ohkami, and C. Murakami, "On Stability of Magnetically Suspended Rotor at High Rotational Speed," Presented at the Aerospace Sciences Meeting, Reno, NV, January 1989.

17. Meeks, C., "Trends in Magnetic Bearing Design," Paper presented at Naval Sea Systems Command Magnetic Bearing Forum, Washington, D.C., July 1989.

18. Sortore, C. K., P. E. Allaire, E. H. Maslen, R. R. Humphris, and P. A. Studer, "Design of Permanent Magnet Biased Magnetic Bearings for a Flexible Rotor," presented at the 44th MFPG Meeting, Virginia Beach, VA, April 2–5, 1990.

19. Humphris, R. R., R. D. Kelm, D. W. Lewis and P. E. Allaire, "Effect of Control Algorithms on Magnetic Journal Bearing Properties," Journal of Engr. for Gas Turbines and Power, Vol. 108, October 1986.

20. Hebbale, K., "A Theoretical Model for the Study of Nonlinear Dynamics of Magnetic Bearings," Master of Science Thesis, Cornell University, January 1985.

Appendix A. Energy Derivation of Bearing Forces

The force generated by magnetic actuators is determined by the sensitivity of the flux density in the circuit to variations in position of the supported structure. This description of the magnetic effect is useful in analyzing the behavior of complex magnetic circuits such as permanent magnet biased actuators. A variety of researchers have employed such an analysis, producing results identical to those based on simpler approaches for simple magnetic circuits [7,18,20]. The analysis is based on a conventional energy variation argument: the magnetic circuit will tend toward a configuration which minimizes its potential energy. The mechanism which produces this tendency is called a "force". Thus, if the magnetic circuit is lossless so that the magnetic energy represents a potential function, the force is described by

$$\underline{f} \equiv -\nabla W_m \tag{A.1}$$

where W_m is the total energy contained in the magnetic field generated by the magnetic circuit and the gradient operator is with respect to configuration space. If the position of the supported structure relative to the magnetic circuit is

$$\underline{s} = x\,\underline{i} + y\,\underline{j} + z\,\underline{k} \tag{A.2}$$

then the force acting on the structure is

$$\underline{f} \equiv -\left\{ \frac{\partial}{\partial x} W_m\,\underline{i} + \frac{\partial}{\partial y} W_m\,\underline{j} + \frac{\partial}{\partial z} W_m\,\underline{k} \right\} \tag{A.3}$$

For the general, nonlinear magnetic circuit, the total energy required to take the field distribution from some nominal state, B_o and H_o, to some other state, B and H is

$$W_m = -\int_{\infty} \int_{B_o}^{B} \underline{H} \cdot d\underline{B}\, dv \tag{A.4}$$

The volume integral is computed over all of space. Assume that the induction, $\underline{B}$, is an explicit function of the variable x which partially describes the position of the supported object and the change from the initial state to some other state is caused entirely by varying x. Then

$$\begin{aligned} f_x\Big|_{H=H_o,B=B_o} &= \frac{\partial}{\partial x} \int_{\infty} \int_{B_o}^{B} \underline{H} \cdot d\underline{B}\, dv \\ &= \frac{\partial}{\partial x} \int_{\infty} \int_{x_o}^{x} \underline{H} \cdot \frac{\partial}{\partial x}\underline{B}\, dx\, dv \end{aligned} \tag{A.5}$$

or,

$$\begin{aligned} f_x = \int_{\infty} \underline{H_o} \cdot \frac{\partial}{\partial x}\underline{B}\Big|_{H=H_o,B=B_o} dv \\ + \frac{\partial}{\partial x} \int_{\infty} \underline{H_o} \cdot \underline{B_o}\, dv \end{aligned} \tag{A.6}$$

Similar expressions describe the forces in the y and z directions. Equation (A.6) forms the basis for computing the forces in the fairly complicated magnetic circuits which comprise permanent magnet biased magnetic bearings.

For design purposes, it will be convenient to compute the forces using a crude finite element method, where it is assumed that the magnetic flux is confined to the physical structure of the magnetic circuit and simply

described air gap volumes. In making this assumption, leakage and fringing effects are neglected. These effects can be included in a more detailed analysis where some estimate of the shape of finite fringing and leakage volumes is determined and added into the circuit description as paths parallel to those passing through the structure. Such refinements improve the accuracy of the performance prediction, but complicate the analysis and tend to obscure the design dependent effects which are to be illustrated. With these limitations in mind, the integral over all space of (A.6) can be written as a sum over the various components of the circuit.

In the air gaps, the relationship between $\underline{H}$ and $\underline{B}$ is linear:

$$\underline{B}_{gap} = \mu_o \underline{H}_{gap} \tag{A.7}$$

Similarly, if the magnetic induction in the iron stays well below the saturation level, the relationship in the iron is similar, scaled by a large (~5000) relative permeability, μ_r:

$$\underline{B}_{iron} = \mu_o \mu_r \underline{H}_{iron} \tag{A.8}$$

The relationship between $\underline{B}$ and $\underline{H}$ in the permanent magnets is quite nonlinear, but it does have the property that $\underline{B}$ and $\underline{H}$ are parallel with opposite sense.

If it is further assumed that each of the components can be broken into a set of sections throughout whose volumes the induction is fairly constant, then (A.6) becomes

$$f_x = \frac{1}{2\mu_o}\sum_{i=1}^{gaps}\frac{\partial}{\partial x}\left\{B_i^2 v_i\right\} + \frac{1}{2\mu_o}\sum_{i=1}^{legs}\frac{1}{\mu_{r_i}} v_i \frac{\partial}{\partial x} B_i^2 + \sum_{i=1}^{magnets} H_i v_i \frac{\partial}{\partial x} B_i \tag{A.9}$$

where the volumes of the iron and permanent magnets have been assumed to be fixed. The scalars B_i and H_i have replaced the corresponding vector quantities because, if the field varies slowly in time, then the two vectors are always parallel: in the iron and air gaps, the vectors point in the same direction whereas in the permanent magnet, they point in opposite directions.

For a well designed magnetic circuit, the flux density in the permanent magnets will be fairly independent of the position of the supported object. Further, the length of the iron paths will be substantially less than μ_r times the length of the air gaps, so (A.9) is dominated by the first term. Neglecting the less significant terms and interchanging the order of summation and differentiation produces

$$f_x \cong \frac{\partial}{\partial x}\frac{1}{2\mu_o}\sum_{i=1}^{gaps} B_i^2 v_i \tag{A.10}$$

The magnetic induction, B, in the air gaps is found from Ampere's circuital law:

$$\oint \underline{H}\cdot d\underline{l} = \iint \underline{J}\cdot d\underline{a} \tag{A.11}$$

which states that the line integral of the magnetic field strength around any closed path is equal to the integral over the enclosed area of the current density in that area. For magnetic circuits whose fields are modulated by winding wire coils around various legs of the circuit and applying currents to these legs, the area integral simply becomes a measure of the total current linked by the path of the line integral. Thus,

$$\oint \underline{H}\cdot d\underline{l} = NI \tag{A.12}$$

where N is the number of wire turns enclosed by the path and I is the current in the wire.

Equation (A.12) can be discretized for the crude finite element approach of this discussion if it is assumed that each element of the magnetic circuit has a characteristic length in the direction of $\underline{H}$ and a characteristic area normal to $\underline{H}$. In this manner, each closed path in the magnetic circuit is governed by

$$\sum_{i=1}^{n} H_i l_i = NI \tag{A.13}$$

where n is the number of elements in the path. If each path contains p iron legs, a air gaps, and m permanent magnets, then (A.13) can be broken into

$$\frac{1}{\mu_o\mu_r}\sum_{i=1}^{p} B_i l_i + \frac{1}{\mu_o}\sum_{i=1}^{a} B_i l_i - \sum_{i=1}^{m} H_i l_i = NI \tag{A.14}$$

Note that the sense of the integral path and the H vector are opposite in the permanent magnets, hence the minus sign preceding the permanent magnet term in (A.14). Further simplification is possible if, consistent with (A.10), the loss in the iron due to finite μ_r is neglected. This produces

$$\frac{1}{\mu_o}\sum_{i=1}^{a} B_i l_i = \sum_{i=1}^{m} H_i l_i + NI \tag{A.15}$$

One further relation is generally required to compute the induction in the gaps. This is Maxwell's divergence theorem which states that

$$\underline{\nabla}\cdot\underline{B} = 0 \tag{A.16}$$

This means that there are no sources or sinks of induction. Practically, it implies that the total flux, Φ, at any node of the magnetic circuit is zero. The flux, Φ, is simply the integral of $\underline{B}\cdot d\underline{a}$ over any surface. In the analysis presented here, it is assumed that $\underline{B}$ is uniform

across any given crossection of the circuit taken normal to $\underline{B}$. Thus, for a fixed element of the circuit,

$$\Phi_i = B_i A_i \qquad \text{(A.17)}$$

For a node of the circuit connected to e elements, (A.16) implies

$$\boxed{\sum_{i=1}^{e} \Phi_i = 0} \qquad \text{(A.18)}$$

where the sense of Φ_i is taken relative to the node: flux into the node is taken as positive while flux out of the node is taken as negative.

Equations (A.15) and (A.18) together with the nonlinear B–H relationship for any permanent magnets in the circuit, define a complete set of governing equations for the inductions in each of the circuit elements. The nonlinear nature of the permanent magnets requires an iterative solution for the resulting network equation, but the solution is generally fairly easy to obtain. Once the inductions have been computed, equation (A.10) can be evaluated for each direction to determine the bearing forces.

As an example, consider the magnetic circuit of Figure A.1.

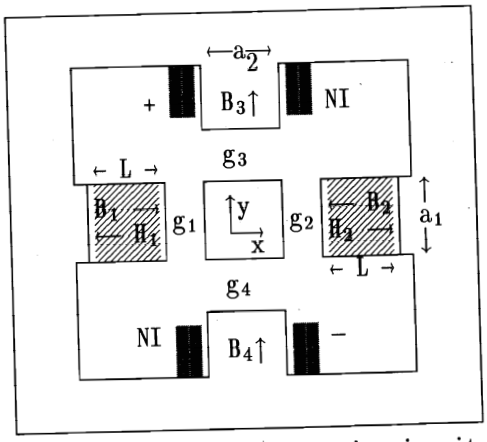

Figure A.1: simple magnetic circuit

The position of the suspended object is given by (x,y). The air gaps have lengths g_1, g_2, g_3, and g_4 given by

$$g_1 = g_a + x\ ;\ g_2 = g_a - x\ ;\ g_3 = g_b - y\ ;\ g_4 = g_b + y$$

Permanent magnets are indicated by the shaded regions ▨ and wire coils are indicated by ▮. The coils have N turns and the current direction is such that a positive I in either of the coils will tend to produce positive B_3 and B_4.

Three independent loop paths can be found to produce via (A.15) the equations

$$B_3 g_3/\mu_0 + B_4 g_4/\mu_0 = 2NI \qquad \text{(A.19)}$$

$$B_1 g_1 + B_2 g_2 = LH_1 - LH_2 \qquad \text{(A.20)}$$

$$B_1 g_1/\mu_0 + B_3 g_3/\mu_0 = LH_1 + NI \qquad \text{(A.21)}$$

Equation (A.18) gives, for the fluxes entering the supported object,

$$B_1 a_1 + B_4 a_2 - B_2 a_1 - B_3 a_2 = 0 \qquad \text{(A.22)}$$

These equations may be summarized by

$$\begin{bmatrix} a_1 & -a_1 & -a_2 & a_2 \\ g_1 & g_2 & 0 & 0 \\ g_1 & 0 & g_3 & 0 \\ 0 & 0 & g_3 & g_4 \end{bmatrix} \begin{Bmatrix} B_1 \\ B_2 \\ B_3 \\ B_4 \end{Bmatrix} = \begin{Bmatrix} 0 \\ \mu_0 L(H_1 - H_2) \\ \mu_0(LH_1 + NI) \\ 2\mu_0 N I \end{Bmatrix} \qquad \text{(A.23)}$$

subject to

$$B_1 = f(H_1) \qquad \text{(A.24)}$$

$$B_2 = f(H_2) \qquad \text{(A.25)}$$

where these latter two functions describe the magnetization curve for the permanent magnet material.

These last three equations must be solved iteratively because of the nonlinearity of (A.24) and (A.25): these functions will typically be specified by an empirical magnetization curve. A symbolic solution to (A.23) was generated using MACSYMA. The resulting expressions were substituted into (A.10) and the forces in the x and y directions were computed to be

$$f_x\big|_{x=0,y=0} = \mu_0 \frac{a_1 a_2 (H_2^2 - H_1^2) L^2}{2g_a(g_a + g_b)} \qquad \text{(A.26)}$$

$$f_y\big|_{x=0,y=0} = \mu_0 \frac{a_1 a_2 (H_1 + H_2) LNI}{g_b(a_1 g_b + a_2 g_a)} \qquad \text{(A.27)}$$

The force in the x direction is independent of the coil current. If $H_1 = H_2$, f_x is zero when the object is centered. The force in the y direction is linear in the current, I. Equation (A.27) illustrates that the magnetization force of the permanent magnets determines the effectiveness of variations in I.

Acknowledgements

The authors would like to thank the Center for Computer Aided Engineering of the Center for Innovative Technology of the Commonwealth of Virginia for partial support of this work. This work was based on research supported in part by a National Science Foundation Graduate Fellowship. Any opinions, findings, conclusions or recommendations expressed in this publication are those of the authors and do not necessarily reflect the views of the National Science Foundation.